Simulation Modeling in Dosimetry

Aleksei Zhdanov
Ural Federal University named after the first President of Russia B. N. Yeltsin,
Yekaterinburg, Russian Federation
jjj1994@yandex.ru

Leonid Dorosinskiy
Ural Federal University named after the first President of Russia B. N. Yeltsin,
Yekaterinburg, Russian Federation
l.dorosinsky@mail.ru

Abstract

In this article, we present simulation modeling in dosimetry based on three experiments: dose measurement, using VERO Linear Accelerator, with different depth of solid water phantom, different dose receivers (ionization chamber and radiographic film), and different field sizes, in order to study the influential factors on the delivered dose. We present the results of the experiments, and explain the relationship between fitting result and theoretical model. Finally, we will discuss the influence of different factors on the delivered dose.

1 Introduction

1.1 Linear Accelerator

Linear accelerator (LINAC), is a device that uses high Radio-Frequency (RF) electromagnetic waves to accelerate charged particles (i.e. electrons) to high energies in a linear path, inside a cavity (to add energy to electron) and wave guide (to guide electron acceleration path). Because of the feasibility to produce beams with accuracy and efficiency, LINAC is the most common device to treat cancer with external beam irradiation in clinic.

The LINAC gantry, which consist of waveguide and accelerator (with cavity inside), bending magnet, target and other beam accessories. The resonating cavity frequency of medical LINACs is about 3 billion Hertz (cycles/sec). The LINAC uses microwave technology to accelerate electrons in a part
of the LINAC called waveguide, then allows these electrons to collide with a heavy metal target. As a result of these collisions, high energy X-Rays (Photons) are produced from the target.

These high energy photons will be directed to the patient's tumor and shaped by Multi-leaf collimator (MLC) as they exit the LINAC to conform to the shape of the tumor. Also radiation can be delivered to the tumor from any angle by rotating the gantry and moving the treatment table. In this article we use a Linear Accelerator (LINAC) 6 MV by MHI (Mitsubishi Heavy Industries Ltd.) to do experiments Fig.1. [1]

1.2 Interaction of Photon Beams with Tissue

Photon beam, as the name indicates, consists of photons with high energy, in which photons are individual units of energy. As an x-ray beam or gamma radiation passes through an object, three possible interactions await each photon:

1. It can penetrate the section of matter without interacting and photon scattering possibilities: Thompson, Compton, Rayleigh, photoelectric and pair productions. These interactions are contribute to dose deposition in the matter.
2. It can interact with the matter and be completely absorbed by depositing its energy.

3. It can interact and be scattered or deflected from its original direction and deposit part of its energy, and photon scattering possibilities: Thompson, Compton, Rayleigh, photoelectric and pair productions. These interactions are contribute to dose deposition in the matter. [2]

Figure 1: LINAC 6 MV by MHI

1.3 Tissue Maximum Ratio (TMR) and Percent Depth Dose (PDD)

In dosimetry, Tissue maximum ratio (TMR) and percent depth dose (PDD) are frequently used dosimetric quantities. PDD is defined as follows:

$$PDD(z, A, f, hv) = 100\, D_Q/D_P = 100\, \dot{D}_Q/\dot{D}_P \quad (1)$$

Where D_Q and $\dot{D}_Q$ are dose and dose rate at point Q, as shown in Fig.3 in the central axis, similarly D_P and $\dot{D}_P$ are dose and dose rate at point P, whose depth is z_{max} in the central axis. Point Q is an arbitrary point at depth z in the central axis, and P represents reference point at $z = z_{max}$ in the central axis. Besides depth z, three parameters determine PDD: field size A, SSD (source surface distance, also denoted as f, and photon beam energy hv.

TMR is a special case of TPR (tissue phantom ratio), and TPR is defined as follows:

$$TPR(z, A_Q, hv) = D_Q/D_{Qref} = \dot{D}_Q/\dot{D}_{Qref} \quad (2)$$

Where D_{Qref} and $\dot{D}_{Qref}$ are dose and dose rate at a reference depth z_{ref} in the central axis, and for TMR, the reference distance is the depth of dose maximum z_{max}, so TMR is defined as follows:

$$TMR(z, A_Q, hv) = D_Q/D_{Qmax} = \dot{D}_Q/\dot{D}_{Qmax} \quad (3)$$

1.4 Radiation Dosimeter

A radiation dosimeter is a device, instrument or system that measures or evaluates, either directly or indirectly, the quantities of ionized radiation. In this article, we introduce two kinds of dosimeters, ionization chamber and radiographic film.

Ionization chamber is basically a gas filled cavity surrounded by a conductive outer wall and having a central collecting electrode. The vent functions of the chamber equalizes the environmental change of air outside the chamber with the air inside the chamber. Measurements with the air vented ionization chamber requires temperature and pressure correction to account for the change in the mass of air in the chamber volume, which changes with the ambient temperature and pressure. [3]

Unlike ionization chamber, radiographic film detects dosimetry based on chemical property. Unexposed film consists of a base of thin plastic layer with a radiation sensitive emulsion coated uniformly on one or both sides. Ionization of irradiation-sensitive grains forms a latent image in the film, which can be processed by scanner as optical density (OD), thus OD is a function of dose and can be used to measure relative dose.

1.5 Output Factor

Because of the use of multi-leaf collimator (MLC), not all dose delivered by LINAC can reach patient. The output factor for a given energy is the ratio of the dose for any specific field size to the dose for a 10 by 10 cm^2 reference applicator, both measured at z_{max} in a phantom.

2 Method and Material

2.1 Water Phantom

Water phantom is designed for absolute dose measurements of photon beams with horizontal beam incidence. Furthermore, it is suitable for combination with dosimeters and make the following calibration of ionization chambers used in radiation therapy feasible. The phantom design allows cross calibration of a field ionization chamber against a calibrated reference chamber at the users facility. [4]

A water phantom has two reasons to use: the first reason is water has similar interaction with soft tissue or muscle since, water has the closest electron density with tissue. The second reason for choosing water as phantom material is that it is universally available with reproducible radiation properties.

Solid dry phantoms is tissue or water equivalent, that has similar electron density with water.

In this article we used the solid water phantom, which is shown in Fig.2.

Figure 2: Solid water slabs that used as phantom in the experiment

2.2 Comparison of Dose Measurement with Constant SSD and SAD

In this article, we use ionization chamber for comparison the dose measurement of constant SDD and SAD as in Fig.3. We choose 6 MV beams at field size a 10 by 10 $cm^2$and 100MU.

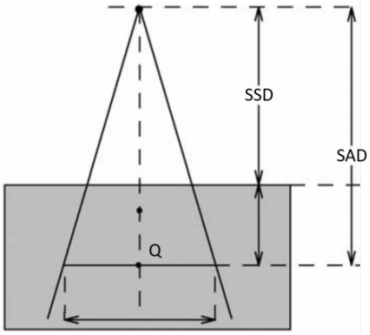

Figure 3: Illustration of SSD and SAD [3]

For experiment with constant SSD, we set the distance from beam source to solid water surface to be constant (1m is the machine isocenter), and change beam depth by adding and removing solid-water slabs (every single solid-water slab

provides the same attenuation as fluid water of 1cm). In order to maintain the constant distance, we modify the height of table every time, we add new slab (only in PDD setting).

For experiment with constant SAD, general setting is similar to that of PDD experiment, and the difference is that we constrain the distance from beam source to the center of ionization center is constant, and variation of water depth is also accomplished by adding and removing solid-water slabs over the ionization chamber. For both dose measurements (PDD,TMR), we choose equivalent water depth from 1cm to 10cm, with general variation of 1cm.

2.3 Film Calibration

To compare different dose response of ionization chamber and radiographic film, we repeat dosimetric measurement with constant SSD with EBT radiographic film as detector, and other parameters are the same (6MV beam, 4cm*4cm field size, 6 different values of MU). We place detector film in between two solid water slabs (PDD setting).

We exposed the film to six different dose values, we choose different values of monitor units (86, 260, 346, 519, 692, and 865 MU). The result represents the relationship between the monitor unit values and delivered dose. The result is film with six different areas with different dose values, so we extract from the six areas of the film the optical density values (OD). Next step is to estimate a function which represents the relation between the optical density (OD) and the delivered dose. The estimated curve is the key for our report because it is the reference to estimate the doses of the other tasks and verify our calculations. We fit the data to rational polynomial function as follows:

General model Rat21:

$$f(x) = (p_1x^2 + p_2x + p_3)/(x + q_1) \tag{4}$$

$$p_1 = 6104; p_2 = -4696; p_3 = 162.8; q_1 = -0.7121;$$

The polynomial nominator is a second degree and the denominator is a first degree, which fit the best the data. The evaluation of this polynomial is as the following: Goodness of fit: SSE: 1.02e+04, R-square: 0.9993, Adjusted R-square: 0.9981, RMSE: 71.41.

2.4 The Effect of Field Size on the Dose Using Ionization Chamber

We measure the dose deposited by a photon beam for different quadratic field sizes (2*2, 4*4, 5*5, 7*7, 10*10, 12*12, 15*15, and 5*15 cm) using an ionization chamber and PDD setting. We study the relationship between the field size and dose. The dependence between field size and dose is proportional that when the field size increases the dose increases.

2.5 Film Dosimetry

We measure the dose deposited by a photon beam for different quadratic field sizes (2*2, 4*4, 5*5, 7*7, 10*10, 12*12, 15*15, and 5*15 cm) using an ionization chamber and PDD setting. We study the relationship between the field size and dose. The dependence between field size and dose is proportional that when the field size increases the dose increases.

3 Result and Discussion

3.1 Dose Measured with Constant SSD and SAD

Result of two experiment are listed below (Fig.4). We can see that dose curve of constant SSD(source surface distance) and SAD(source to axis distance) share similar trend, that relative dose increases with depth z until it reaches zmax and then decline.used in radiation therapy feasible. The phantom design allows cross calibration of a field ionization chamber against a calibrated reference chamber at the users facility.

In the article, we conduct two measurements using ionization chamber, which set SSD and SAD separately. According to the definition of TMR and PDD, constant SSD means constant z_{max}, so dose measured with constant SSD should represent PDD. Similarly, constant SAD indicates that total dose is constant, which means D_{Qmax} is constant through the experiment, so dose measured with constant SAD can represent the variation of TMR.

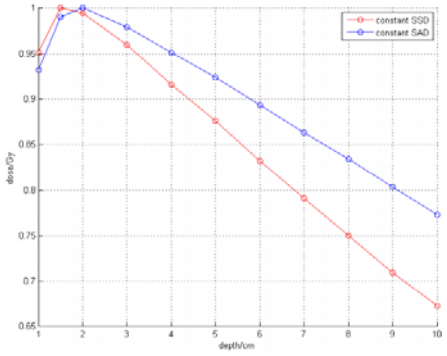

Figure 4: Curve of measured dose

3.2 Relationship between PDD and TMR

As before, doses measured with constant SSD can represent the variation of PDD, and doses measured with constant SAD can represent TMR, so we use doses measured in two separate experiment to study the relationship between PDD and TMR.

According to the property of attenuation along central axis in the slabs, doses of certain depth and from the same source are inversely proportional to the field size at that depth, thus we get:

$$\frac{D_Q}{D_S} = \left(\frac{f + z_{max}}{f + z}\right), z_m ax = 1m \tag{5}$$

Where D_Q and D_S denotes dose at point Q and at the surface of the water slabs, f denotes distance from source to water slab, and z denotes depth of Q. For constant SDD measurement, f is constant and in this experiment:

$$f = 1m \tag{6}$$

$$D_Q = \left(\frac{1}{1+z}\right)^2 D_S$$

And for constant SAD dosimetric measurement, $f + z$ is constant and similarly:

$$f + z = 1m \tag{7}$$

$$D'_Q = \left(\frac{1-z}{1}\right)^2 D'_S = (1-z)^2 D'_S$$

In this case, D_S and D'_S refer to different surfaces and their relationship:

$$\frac{D_S}{D'_S} = \left(\frac{1+z}{1}\right)^2 \tag{8}$$

By displacing D'_S we can get the relationship between D_Q and D'_Q:

$$\frac{D_Q}{D'_Q} = \left(\frac{1}{1-z}\right)^2 \tag{9}$$

From (Fig.5, Table 2), we can see that, within in the error range calibration line fits measurement in the experiment, which support our derivation of relationship between exposure with constant SSD and constant SAD.

Ignoring the effects of point spreading function (PSF), we can also get easily from (9) the relationship between TMR and PDD from this:

$$TMR \approx \frac{PDD}{100}\left(\frac{f+z}{f+z_{max}}\right)^2 \tag{10}$$

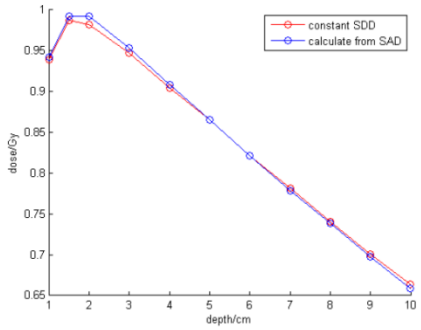

Figure 5: Verification of relationship of TMR and PDD

Table 1: Dose of different depth with constant SSD and SAD

Slabs depth /cm	Dose with constant SSD/Gy	Dose with constant SAD/Gy
10	0.6643	0.7976
9	0.7004	0.8293
8	0.7403	0.8611
7	0.7810	0.8910
6	0.8217	0.9224
5	0.8655	0.9537
4	0.9045	0.9820
3	0.9478	1.0110
2	0.9822	1.0320
1.5	0.8975	1.0220
1	0.9294	0.9616

Table 2: Comparison of Doses with Constant SSD and calculation from (9)

Slabs depth /cm	Dose with constant SSD /Gy	Dose calculated from (9)/Gy	Error /%
10	0.6643	0.6592	0.77
9	0.7004	0.6980	0.34
8	0.7403	0.7383	0.28
7	0.7810	0.7782	0.35
6	0.8217	0.8209	0.09
5	0.8655	0.8650	0.05
4	0.9045	0.9079	0.38
3	0.9478	0.9530	0.54
2	0.9822	0.9919	0.99
1.5	0.9875	0.9920	0.46
1	0.9394	0.9427	0.35

3.3 Film Calibration

We irradiate six different doses to six areas of the film based on six different monitor unites as in Fig.6. We calculate the mean value of each interested area of the film and for the background as well [4]. Then we calculate the optical density (OD) using the equation (11), I represents the mean value of the dose and I0 represents the mean value of the background:

$$OD = \log(\frac{I_0}{I}) \tag{11}$$

Fig.7 shows the dependence between the optical density (OD), and the dose (blue points). We fit a second order polynomial function to the data points, and as we can see the relation between the OD and dose is proportional, when the OD increases the dose increases. Table 3 shows the all the results that we extract from the film. It also presents the error between the delivered dose and the estimated dose.

We perform another experiment to verify the fitted function. We exposed another film to 300 MU as we can see in Fig.8, and we estimate the dose of new film from the fitted function in the previous step. The result is shown in the table 4. We can conclude from the verification step that the function, which we estimate from the six doses, that estimates the relationship between the OD and the dose and the error is 0.71%.

Fig. 7 shows the measurement characteristic of radiographic film. OD of the film is approximately proportional to deposited dose to the area, thus we can tell the dose distribution visually by using radiographic film, though OD is not exactly dose.

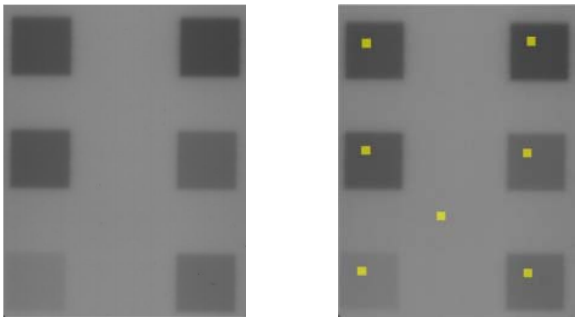

(a) scanned film (b) film with sampling markers

Figure 6: Original film (a) and region we choose for averaging to get mean OD (b)

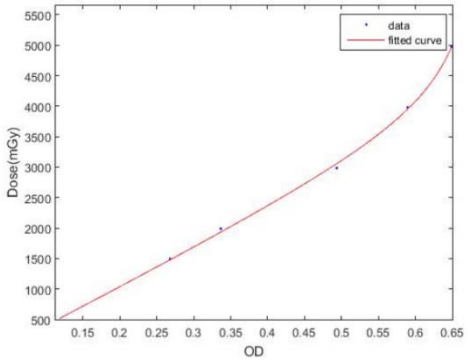

Figure 7: Optical density as a function of dose of a 4x4 cm field size

Table 3: Dose of different monitor units values and the estimated doses from the fitted function

Mean value	OD	Delivered dose /mGy	Estimated dose /mGy	Error /%
30771	0.1190	494.672	522.0628	0.2739
26516	0.2678	1495.52	1478.9	0.1662
24754	0.3366	1990.192	1934.1	0.5613
21157	0.4936	2985.288	3056.9	0.7158
19221	0.5896	3980.384	3950.7	0.2871
18108	0.6492	5497.548	4979.0	0.0350

Table 4: Verifying step for dose of 300 MU value

Mean value	OD	Delivered dose /mGy	Estimated dose /mGy	Error /%
34899	0.3143	1.73	1.7060	0.0240

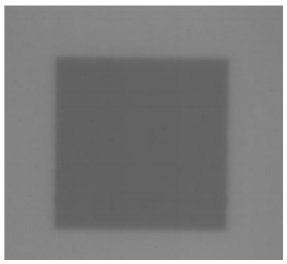

Figure 8: Delivered dose of 300 MU and field size 10 by 10 cm

3.4 The Effect of Field Size on the Dose Using Ionization Chamber

Beams used for radiotherapy have various shapes that usually represent a compromise between the actual target shape and the need for simplicity and efficiency in beam shaping. Four general groups of field shape are used in radiotherapy: square, rectangular, circular and irregular.

We present in this section the result of changing the field size and its effect on the delivered dose. We perform the experiment by varying the field size (2*2, 4*4, 5*5, 7*7, 10*10, 12*12, 15*15, and 5*15 cm) and record the delivered dose of ionization chamber. We notice that with increasing the field size the dose increases as well, and this is because we are increasing the exposed area of radiation, which accumulated into larger dose, which means higher recorded dose as we can see in Fig.9 and table 5. For any arbitrary radiation field an equivalent square may be found, meaning that the arbitrary field and the equivalent square will be characterized with similar beam parameters and functions that are of importance in radiation dosimetry. An arbitrary rectangular field with sides a and b will be approximately equivalent to a square radiation field with sides (a_{eq}) when both fields have the same area/perimeter ratio (Day's rule):

$$\frac{ab}{2(a+b)} = \frac{{a_{eq}}^2}{4a_{eq}} \tag{12}$$

We will discuss based on eq.12, that if we have field size with dimensions 5x20 cm what will be the result?. We can answer this question from the mathematical side. a_{eq} equals to 8 based on eq.12. The area of this field (${a^2}_{eq}$) is 64 cm*cm, then the dose of this field is 648.4269 mGy as it was estimated from Fig.9. If we have field size with dimensions 5x15 cm what will be the result? We can answer this question from the mathematical side. a_{eq} equals to 7.5. The area of this field (${a^2}_{eq}$) is 56.2 cmxcm, then the dose of this field is 650.5464 mGy as it was estimated from Fig.9.

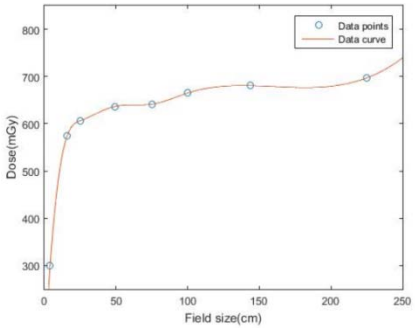

Figure 9: Dose as a function to different field sizes using ionization chamber as detecting device

Fig.10 represents dose depth profile of the film in Fig.8. The result shows the difference of dose values between the delivered dose area (field size 10x10 cm) and the background area.

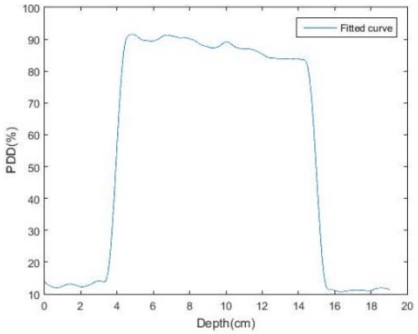

Figure 10: PDD [%] experimental values at different depths (cm) obtained by scanning radiographic film

Table 5: Dose of different field sizes

Field size /cm	Delivered dose /mGy	Estimated dose /mGy	Error /%
4 (2*2)	299.6	348.2	0.4863
16 (4*4)	575.2	516.4	0.5872
25 (5*5)	606.3	597.3	0.0892
49 (7*7)	636.4	651.9	0.1552
75 (5*15)	641.3	647.5	0.0629
100 (10*10)	665.0	661.9	0.0307
144 (12*12)	680.6	680.8	0.0025
225 (15*15)	697.0	697.0	0.0003

3.5 Film Calibration

We measure the calibration curve for film dosimetry using 10*10 field size in 10 cm depth (solid water) after rotating the source of radiation 90 degree around the film. The idea of this setup is to analyze the dose distribution in the film and see the difference between the film outside the solid water slabs and inside them and compare it to the result of ionization chamber using PDD setting. We notice that the dose is increasing from the starting point of the film until it reaches the maximum value. Then the curve decreases because the last part of the film exposed by less radiation as we can see in Fig.11. We use smoothing spline function for the fitting step and it is f1(x) = piecewise polynomial computed from p (coefficient structure p=0.9357) and after that we performed smoothing step. In Fig.12, we can see the PDD values of ionization chamber and radiographic film in the same figure.

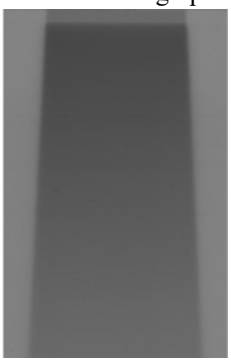

Figure 11: Dose distribution of radiographic film after being exposed to radiation along 90 degree

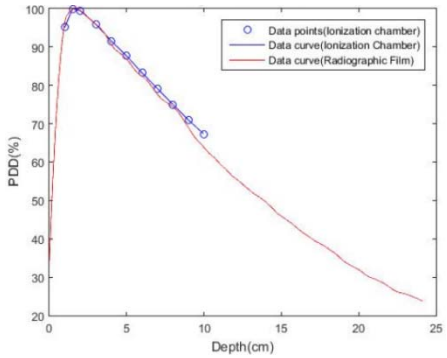

Figure 12: PDD [%] experimental values at different depths (cm) obtained by scanning radiographic film and ionization chamber

We verify the result of the radiographic film and ionization chamber as we can see in Fig.12 by calculating the error between the two graphs for different depth values (1, 1.5, 2, 3, 4, 5, 6, 7, 8, 9, and 10 cm). The maximum error is 3.49% as we can see in Table 6, which is acceptable based on the chosen curves fitting.

Table 6: Dose of difference between film and ionization chamber from calibration curve

Depth /cm	Dose of the film /%	Dose of ionization chamber /%	Error /%
1	96.5127	96.2887	0.2240
1.5	99.8497	98.6223	1.2273
2	99.5677	99.2651	0.3026
3	96.0309	96.2923	0.2614
4	90.6436	91.7691	1.1255
5	86.7252	87.5395	0.8142
6	82.3835	83.2584	0.8749
7	77.5859	79.0710	1.4851
8	74.3751	74.9540	0.5789
9	68.8769	70.9698	2.0929
10	63.7483	67.2458	3.4975

4 Conclusion

During radiation, the absorbed dose in the patient varies with depth. This variation depends on many conditions: beam energy, depth, field size, distance from source, and beam collimation system. These parameters must be considered when calculating the dose in the patient. Percentage Depth Dose (PDD) and Tissue Maximum Ratio (TMR) are dosimetric quantities defined for this purpose. Percentage depth dose increases with increased SSD because as the SSD is increased, the volume of the area irradiated is decreased and the interactions are more concentrated.It is more practical to use dosimetric quantities that are independent on SSD such as TMR for isocentric treatment planning. [5]

For a small field size, the contribution of the scattered photons to the depth dose in this case is negligibly small or 0. But as the field size is increased, the contribution of the scattered radiation to the absorbed dose increases. Because this increase in scattered dose is greater at larger depths, the percent depth dose increases with increasing field size.

5 Acknowledgements

All dates and images were taken by Brainlab Vero Linac of Erlangen University Clinic. The experiments which is shown in this article was supported by Prof. Dr. rer. nat. Christoph Bert of Friedrich-Alexander University Erlangen-Nürnberg, Erlangen.

References

1. P. Sprawls. Physical Principles of Medical Imaging { Volume 545 / Aspen Publishers, 1987.
2. J.P. Seuntjens, W. Strydom, K.R. Shortt. Review of Radiation Oncology Physics: A Handbook for Teachers and Students { Volume 132 / IAEA, 2006.
3. K. Kainz. Radiation oncology physics: a handbook for teachers and students { Volume 657 / Medical Physics, 2006.
4. Khan, M. Faiz. Physics of Radiation Therapy { Volume 3 / Lippincott Williams & Wilkins, 2003.
5. M.Y. Abdallah, M.A. Boshara.Assessment of field size on radiotherapy machines using texture analysis { Volume 10 / Sudan Medical Monitor. Published by Wolters Kluwer, 2017